Carbon Letters (2023) 33:1445–1460
https://doi.org/10.1007/s42823-022-00452-5

Online ISSN 2233-4998
Print ISSN 1976-4251

ORIGINAL ARTICLE

Treatment of wastewater containing organic pollutants in the presence of N-doped graphitic carbon and Co_3O_4/peroxymonosulfate

Hakkı Türker Akçay[1] · Adem Demir[2] · Zehra Özçifçi[1] · Tuğrul Yumak[3] · Turgut Keleş[2]

Received: 20 September 2022 / Revised: 14 December 2022 / Accepted: 20 December 2022 / Published online: 2 January 2023

Abstract

The disposal of organic pollutants is one of the important research topics. Some of the studies in this field are based on the degradation of organic pollutants with a catalytic agent. The cobalt tetraoxide/peroxymonosulfate system is an important catalytic system used for the radical degradation of organic pollutants. To increase the catalytic efficiency of such reactions, graphitization of activated carbon used as a support solid and nitrogen doping to the carbon structure are commonly used methods. In this study, cobalt tetraoxide production, N-doping and graphitization were carried out in a single step by heat treatment of activated carbon doped with the phthlocyanine cobalt (II) complex. The catalytic performance of the catalyst/peroxymonosulfate system was investigated by changing the pH, catalyst, and PMS concentration parameters on rhodamine B and 1,3,5 trichlorophenol, which were used as models. It was seen that the catalysts had 97% activity on rhodamine B in 16 min and 100% on 1,3,5 trichlorophenol in 6 min. It was observed that the catalysts continued to show high catalytic activity for five cycles in reusability studies and had a very low cobalt leaching rate. These results are in good agreement with previously published studies. In line with these results, the synthesized N-doped graphitic carbon/Co_3O_4 catalyst can be used as an effective catalyst for wastewater treatments.

Graphical abstract

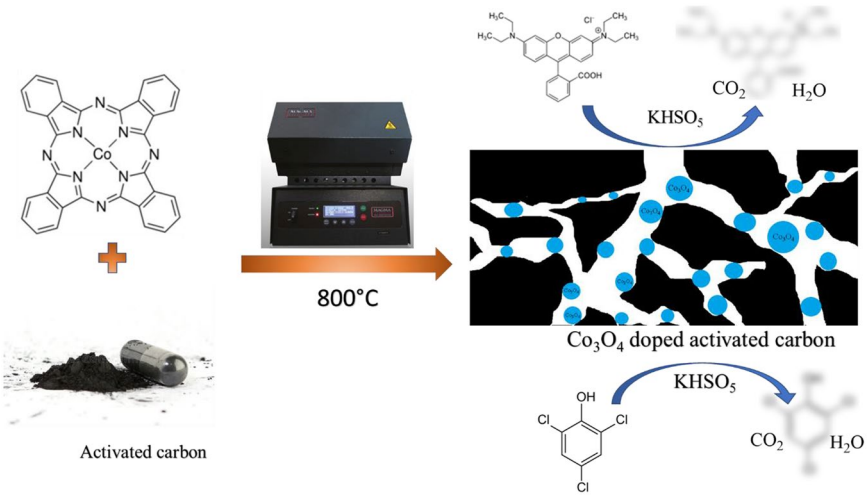

Keywords Peroxymonosulfate · Rhodamine B · 2,4,6-Trichlorophenol · Catalytic degradation · Water treatment

✉ Turgut Keleş
turgut.keles@erdogan.edu.tr

Extended author information available on the last page of the article

Abbreviations

Co3O4	Cobaltite
AC	Activated carbon

RhB	Rhodamine B
2,4,6-TCP	2,4,6-Trichlorophenol
PMS	Peroxymonosulfate
PS	Persulfate
XRD	X-ray powder diffraction
SEM	Scanning electron microscope
FTIR	Fourier transform-infrared
BET	Brunauer–Emmett–Teller
eV	Electron volt
OH·	Hydroxyl radical
$SO_4^{\cdot -}$	Sulfate radical
$O_2^{\cdot -}$	Peroxide radical
$^1O_2$	Singlet oxygen
Co	Cobalt
TEM	Transmission electron microscopy
THF	Tetrahydrofuran
TBA	*tert*-Butyl alcohol
p-BQ	*p*-Benzoquinone
QS-DFT	Quenched solid density functional theory
BJH	Barret–Joyner–Halende
N_2	Nitrogen
nm	Nanometer
C_o	Initial concentration
C_t	Concentration at time
k	Fisrt-order reaction constant
EtOH	Ethanol
TOC	Total organic carbon

1 Introduction

Rhodamine B (RhB) is widely used in textile, leather, agriculture, food, and dyeing, while 2,4,6-trichlorophenol (TCP) is largely employed in the fungicide, herbicide, insecticide, and pharmaceutical industries [1] The release of these pollutants to groundwater is a major problem due to negative effects on human health including cancer, skin and eye defects, and respiratory and cardiovascular disorders. Moreover, it is known that the pollution of water resulting from these pollutants causes a devastating effect, threatening the whole life of the ecosystem [2]. In addition, the importance of the water needs of the increasing world population has been increasing day by day and access to clean water resources has become increasingly difficult. These chemical wastes are removed by different processes including adsorption [3], photocatalysis [4], chemical oxidation, Fenton-like methods [5], and electrochemical [6] and advanced oxidation processes (AOPs) [7]. AOPs have recently gained interest among these methods because of higher degradation yields and shorter process times [8].

The catalytic system containing transition metals and peroxymonosulfate, (PMS)/persulfate (PS), is one of the AOP systems that has significant advantages such as shorter reaction time, higher degradation efficiency, and lower cost in the degradation of organic pollutants [9]. The mechanism of action of these catalytic systems is based on the formation of the sulfate radical ($SO4^{\cdot -}$). PMS-based catalytic systems have higher performance in environments with variable pH values such as wastewater, due to the sulfate radical's ability to operate in a wider pH range, high redox potential, and high lifetime, compared to Fenton-based catalysts producing hydroxide radical (OH·) [10]. The mechanism of action of this catalytic system is based on the formation of the sulfate radical ($SO4^{\cdot -}$) by activation of the UV irradiation [11], carbon-based materials [12] and transition metal ions, or metal oxide analogs [13].

There are many publications in the literature on the use of metal/metal oxide catalysts doped on carbon support solids in the peroxymonosulfate system. Some of the materials produced in these studies are only obtained by metal/metal oxide doping into activated carbon structures, while another part is on heteroatom doping or the use of graphitic materials to increase the catalytic activity. Since the catalytic systems used in the literature and the model pollutants used are different, it was not possible to make a complete comparison of the catalytic system used in this study. In a study by Ren et al. in 2021, the catalytic activity of metallic cobalt doped on the carbon matrix with peroxymonosulfate on ibuprofen was investigated. In the study, it was observed that 10 mgL^{-1} ibuprofen was completely degraded in 60 min. Although the study reflects the average results in terms of reaction rate, and it is seen that the catalyst works in a narrow pH range such as 5–7.5. This may create a disadvantage, as it requires pH adjustment in studies with real samples [14]. In a study conducted by Hengduo et al. in 2020, the catalytic activity of the Co_3O_4-doped biochar/PMS system on three model compounds (chloramphenicol—CAP, florfenicol—FF, thiamphenicol—TAP) was investigated. The study is important in that it shows that Co_3O_4 alone has lower efficiency under the same catalytic conditions compared to the biochar-doped Co_3O_4 catalyst. This confirms that porous carbon materials increase catalytic efficiency by forming active centers. In the study, the degradation rate of these three model compounds at 10 mM PMS, 0.4 gL^{-1} catalyst concentration and 10 min reaction time were 97.6 ± 1.2%, 71.8% ± 1.0%, and 86.4% ± 1%, respectively [15]. Another study showing that porous carbon structures increase catalytic efficiency was done by Zhao et al. in 2019. In this study, unlike the previous ones, the cobalt compound prepared in an egg white matrix was subjected to heat treatment to obtain a mesoporous and relatively high surface area Co_3O_4 catalyst compared to metal oxides. In the study, 2-s-butyl-4,6-dinitrophenol was used as a model compound at a concentration of 20 mgL^{-1}, and a degradation rate of 97.56% was obtained at the end of the reaction time of 60 min (catalyst concentration: 0.1 gL^{-1}, PMS: 0.5 $mmolL^{-1}$). Although the contribution of porosity

to the catalytic efficiency is emphasized in the study, it is seen that the catalytic activity time is extended up to 60 min because metal oxides are limited in terms of surface area and total pore volume compared to activated carbons. On the other hand, the fact that the catalyst continued to show high catalytic activity with a very low leaching rate for five cycles stood out as an advantage pointing to the stability of the one-component catalyst [16].

Two main effects come to the fore in the improvement of the catalytic properties of the substances: graphitization and heteroatom doping. Graphitization and nitrogen doping can enhance the charge transfer efficiency of carbon-based catalysts. Nitrogen-doped activated carbons can be effective in degrading organic pollutants in the presence of PMS in two main ways. The first of these is that the free electron pair on the nitrogen takes part in the electron transfer mechanism from the pollutant to the PMS, and the other is that it creates active centers in the carbon material for the degradation of the organic pollutant. In the literature, some studies have used nitrogen-doped catalysts containing carbon-based planar structures and based on PMS activation. In a study by Zeng et al. in 2016, the prepared polydopamine cobalt(II) complex was doped on graphene oxide and exposed to heat treatment, and the degradation effect of the obtained nitrogen-doped, graphitic carbon and cobalt(II)-containing catalyst (NRGO@Co) on 4-chlorophenol (4-CP) was investigated. The prepared catalyst degradated 4-CP by 90% in the reaction time of 60 min (catalyst 0.2 g L^{-1}, initial 4-CP 20 mg L^{-1}, PMS 2 g L^{-1}, temperature 298 K). To examine the effect of the components that make up the catalyst, the catalytic performance was investigated by adding cobalt-free NRGO and cobalt nanoparticles separately to the experimental system and it was observed that the catalytic decomposition efficiency decreased below 70% at the same reaction time. This ratio is almost the same as the catalytic efficiency of the NRGO/PMS system prepared without the use of cobalt. Like our present study, it has been shown that metal/metal oxide catalysts increase catalytic activity by creating a synergistic interaction with the matrix [17]. Yi et al., in a study conducted in 2022, calcined the material prepared by the addition of $Co(NO_3)_2$ to the polyvinylpyrrolidone matrix and determined that the obtained catalyst showed approximately 100% degradation in 30 min for 4-nitrophenol (PNP = 0.02 gL^{-1}, catalyst = 0.14 gL^{-1}, PMS = 0.52 gL^{-1}, temperature = 25 ℃, pH = 6.20). In the same study, the catalyst showed close to 100% catalytic activity on rhodamine B in 3 min under the same conditions [18].

The present study aims at the following: (1) to prepare the catalyst in one step and by basic chemical methods, (2) to obtain a high amount of graphitic active centers located in Co3O4 and nitrogen atoms, (3) to obtain micro and mesoporous carbon structures that provide stability and deposition of the radical species formed, (4) to attain a low cobalt leaching rate due to the porosity of the carbon structure and anchoring effect of the nitrogen atoms, (5) to obtain high reusability, and (6) to obtain catalytic activity comparable to similar studies. For these purposes, phthalocyanine, which is a planar molecule containing nitrogen and cobalt atoms, with high thermal stability, is doped with high surface area activated carbon, and a graphite structured catalyst containing porous Co_3O_4 and nitrogen atoms were prepared. After the structure of the prepared catalyst was characterized by XRD, SEM/EDX, TEM, elemental analysis and IR technices, its catalytic effect on rhodamine B and 2,4,6-trichlorophenol as a model compound in the PMS catalytic system for different reaction conditions was investigated.

2 Experimental

2.1 Materials and methods

RhB ($C_{28}H_{31}ClN_2O_3$) ≥ 95%, 2,4,6-trichlorophenol (2,4,6-TCP) 98%, oxone ($2KHSO_5{\cdot}KHSO_4{\cdot}K_2SO_4$) > 95%, phthalonitrile (99%), cobalt (II) chloride (97%), ethanol (99.8%), tetrahydrofuran (THF) ≥ 99.9, *tert*-butyl alcohol (TBA) ≥ 99.5, *p*-benzoquinone (*p*-BQ) ≥ 98 and Trolox 97% were purchased from Sigma-Aldrich. The commercial activated carbon was purchased by a local supplier, and it was dried for 3 h at 120 °C before use. All stock solutions were prepared with deionized water using Human Corporation Zeneer Power 1 water purification instrument.

The XRD spectra were recorded in Rigaku (Japan) smart lab system with TruSpec Micro device (2θ = 2–90°) with the scanning method using Cu–Kα radiation with a wavelength of 1.5408 Å operated at 40 kV, 30 mA. The SEM and EDS images of materials were obtained using a JEOL (Japan). The TEM images of samples were recorded by Hitachi HT-7700 (Japan) equipped with the lanthanum hexaboride electron beam gun with 40–120 eV. The surface area and porosity were studied with a BET analyzer (Quantachrome, USA) by nitrogen adsorption at − 196 °C. The degassing of samples was performed under a vacuum at 105 °C for 15 h before the measurement. The surface area, total pore volume, pore size distribution of AC and Co–AC were calculated by the Brunauer–Emmett–Teller (BET) method, the quenched solid density functional theory (QS-DFT) and Barrett–Joyner–Halenda (BJH) method [19]. The FT-IR spectra of Co–AC for C−H, C−N, C−O, C=N, C=O, NH and OH bending and stretching vibrations were recorded in the Perkin Elmer Spectrum One Spectrometer (USA) in the range of 4000–650 cm^{-1}. Elemental analysis results were obtained with Leco Truspec Micro (USA).

The catalytic activity of Co–AC was determined under different pH, temperature, catalyst and PMS concentrations by using Thermo Scientific Multiskan Go UV/VIS

spectrophotometer (USA) at 554 nm for RhB, but TCP was measured by Thermo Scientific Finnigan HPLC with UV detector at 280 nm. Also, cobalt leaching was analyzed with ICP-OES OPTİMA 7000 DV Perkin Elmer (USA). Moreover, the reusability of catalyst was studied and radical scavenging experiments were applied in the presence of various radical scavengers such as ethanol (EtOH) for $SO_4^{\cdot -}$ and OH·, tert-butanol (TBA) for OH· and *p*-benzoquinone (*p*-BQ) for $O_2^{\cdot -}$, and Trolox was chosen for non-radical trials.

2.2 Preparation of Co–AC catalyst

Cobalt phthalocyanine is synthesized according to the literature [20]. 200 mg phthalocyanine (II) complex and 200 mg commercial activated carbon (AC) were mixed in 50 mL of THF and stirred for 3 days at room temperature. After that, THF was evaporated and the resulting solid was carbonized for 1 h at 800 °C under 100 mL min^{-1} N_2 flowing and then washed with water three times.

2.3 Catalytic performance of Co–AC

To investigate the catalytic performance of Co–AC, the degradation of RhB via PMS was chosen as a model catalytic reaction. The decrease of absorption peak ($\lambda_{max} = 554$ nm) of RhB was monitored with Thermo Scientific Multiskan Go UV/Vis spectrophotometer at 25 °C. While there was no significant change in the absorption peak of RhB without Co–AC, at the end of 30 min of adsorption–desorption time, 15% reduction in the maximum absorption peak in the catalyst system without PMS was observed. The degradation of RhB was measured at 97.07% in 16 min in the experimental system consisting of 12 mgL^{-1} RhB aqueous solution, Co–AC and PMS (150 mgL^{-1} and 90 mgL^{-1}) in Fig. S1 (Supplementary Material). After a certain period of reaction, sample solutions were filtered via syringe with a filter (0.45 µm) and analyzed at 554 nm. For 2,4,6-TCP, the same operations were applied using 150 mgL^{-1} of Co–AC catalyst and 25 mgL^{-1} of the aqueous solution of 2,4,6-TCP and 100% degradation was obtained at the end of 6 min in Fig. S2. The reaction was monitored by HPLC at 280 nm. Under the same steps, the effects of different reaction temperatures, pH values, amounts of PMS, and Co–AC on the catalytic reaction were examined. According to the results, the kinetic parameters of catalytic degradation of RhB and 2,4,6-TCP followed the pseudo-first-order modelas shown in Eq. 1.

$$\mathrm{In}\left(\frac{C}{C_0}\right) = -kt, \tag{1}$$

where "C_0" is the initial concentration of RhB and 2,4,6-TCP, "C" is the concentration at the time "t", and "k" is the first-order reaction rate constant. The kinetic parameters were calculated as in the literature [21]. Thus, the degradation of RhB and 2,4,6-TCP in the presence of Co–AC/PMS was studied in the following experiments.

2.4 Degradation of RhB and 2,4,6-TCP and other catalytic parameter experiments

The catalytic activity of Co–AC was investigated with degradation of RhB in deionized aqueous solutions and the degradation experiments were applied in a 100 mL glass bottle with magnetic stirring at 25 °C. Firstly, the solution of RhB (12 mgL^{-1}) was prepared with deionized water and the initial concentration of Co–AC catalyst was determined as 7.5 mg. The 100 mL of dye solution and 7.5 mg catalyst were vigorously stirred at 25 °C to form an adsorption–desorption equilibrium between Co–AC and RhB and then the degradation reaction was started with 9 mg PMS was added to the reaction mixture. The course of the degradation reaction was monitored by measuring their absorbance at 554 nm and periodically sampling the filtered aliquots from the main solution. To stop the degradation reaction, the catalyst was removed from aliquots by filtering with a 0.45 µm PTFE syringe filter. The absorbance values were recorded by Thermo Scientific Multiskan Go UV/Vis spectrophotometer. The degradation experiments of 2,4,6-TCP were applied similarly to that of RhB. 25 mgL^{-1} 2,4,6-TCP stock solution was prepared and used in 100 mL portions. The 100 mL 2,4,6-TCP solution and 10 mg Co–AC catalyst were incubated by stirring at 25 °C to set the adsorption–desorption equilibrium. After that, 6 mg PMS was added to the reaction media to start the reaction. The course of degradation reaction was monitered as in sampling of degradation of 2,4,6-TCP by HPLC at 280 nm. (The concentration of 2,4,6-TCP was measured by HPLC with C18 column (250 mm × 4.6 nm, 5 µm) and diode-array-detect or, the mobile phase consisted of acetonitrile/water (60:40 volume ratio), 0.1% formic acid and the column flow rate was gone through with 0.6 mL min^{-1}). [22] Moreover, the effects of the catalyst concentration (50–150 mgL^{-1}), PMS concentration (30–120 mgL^{-1}), pH (2–11) and temperature of the solution (25 °C, 35 °C and 45 °C) were studied on the catalytic activity of RhB. Similarly for TCP, PMS concentration was determined in the range of 50–150 mgL^{-1} for catalyst and 30–120 mgL^{-1} for PMS, the range of pH value 2–11 and temperature 25 °C, 35 °C and 45 °C to obtain optimum catalyst efficiency. The reusability experiments of RhB and 2,4,6-TCP were performed by the addition of fresh RhB and 2,4,6-TCP solutions at the end of the first cycle and the same procedure was performed for other cyles. The radical scavenging experiments were studied to distinguish radical species such as $SO_4^{\cdot -}$, OH·, $O_2^{\cdot -}$ and $^1O_2$. The ethanol (EtOH), *tert*-butyl alcohol (TBA), and *p*-benzoquinone

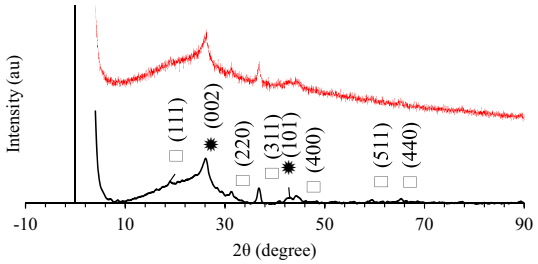

Fig. 1 XRD pattern of Co–AC (red line), normalized and smoothed XRD pattern of Co–AC (black line), (unfilled square: Co3O4 and asterisk: carbon peaks)

(*p*-BQ) were used for quenching $SO_4^{\cdot -}$ or OH·, OH· and $O_2^{\cdot -}$, respectively, as a radical quencher [23]. In addition, Trolox was used for $^1O_2$ quencher [24] according to the determined concentrations in the Co–AC/PMS system.

3 Results and discussion

3.1 Characterization of the Co–AC catalyst

Figure 1 shows the XRD pattern of the Co–AC. The peaks at 2θ, 18.96, 31.32, 36.8, 44.28, 59.50, and 65.34° corresponding to (111), (220), (311), (400), (511) and (440), respectively, are consistent with the standard card JCPDS No. 42–1467 with the lattice constant a = 0.8084 nm (space group Fd-3 m [227]). Also, the peaks observed at 2θ, 26.08° and 42.44°, are attributed to graphite-like structures with hexagonal and cobalt tetraoxide peak and high intensity in the cubic crystal system [25, 26]. The clear XRD pattern of Co–AC shows that there are no impurities in the product. The crystallite (grain) sizes were calculated by Debye–Scherrer equation (Eqs. 2) at 2θ = 36.8°.

$$D = \frac{k\lambda}{\beta_D cos\theta}, \tag{2}$$

where *K* is a constant (ca. 0.9); λ is the X-ray wavelength used in XRD (1.5418 Å); θ is the Bragg angle; β is the pure diffraction broadening of a peak at half-height, that is, broadening due to the crystallite dimensions. The crystallite size of Co_3O_4 calculated by the Scherrer formula is 18.6 nm.

The N_2 adsorption–desorption isotherms of activated carbon and Co–AC in Fig. 2 are assigned to type-II with H4 type hysteresis, with slit shape, commonly observed in activated carbon materials [27]. As can be seen in Table 1, the addition of phthalocyanines cobalt (II) decreases the specific surface area of activated carbon from 904.1 to 256.2 m^2g^{-1}. This is evidence that the phthalocyanine cobalt (II) complex was adsorbed into the micro and mesopores of AC as expected. Probably, in the furnace, the phthalocyanine

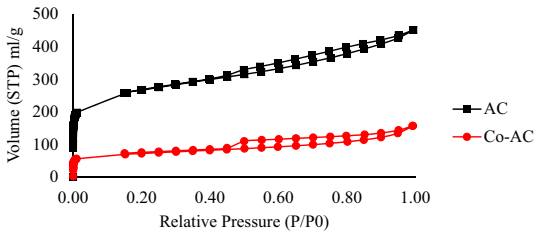

Fig. 2 Adsorption and desorption isotherms of AC and Co–AC

Table 1 Specific surface properties of AC and Co–AC

Sample	BET	BJH	QS-DFT	
	Surface area m^2g^{-1}	Surface area m^2g^{-1}	Pore volume mLg^{-1}	Surface area m^2g^{-1}
AC	904.1	208.8	0.64	1042.4
Co–AC	256.2	114.8	0.215	279.1

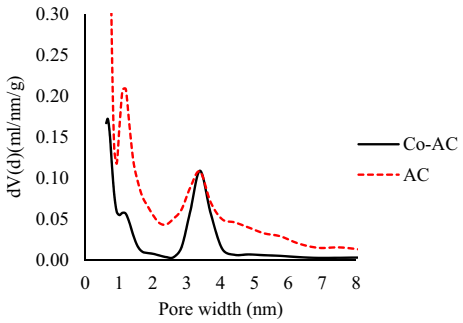

Fig. 3 Pore size distribution of AC and Co–AC determined by the QS-DFT method

ring fused with the functional sites on activated carbon. The specific surface area of activated carbon and Co–AC catalysts was calculated by the BET and QS-DFT methods and determined to be 904.1 and 256.2 m^2g^{-1} for BET and 1042.4 and 279.1 m^2g^{-1} for QS-DFT, respectively [28]. According to the BJH method, the specific surface area of AC and Co–AC was found to be 208.8 and 114.8 m^2g^{-1}, respectively. This situation showed that both AC and Co–AC consisted of both micropores and mesopores. The pore size distribution of the AC and Co–AC calculated by the QS-DFT method in Fig. 3 was consistent with the BJH and QS-DFT values. The total pore volume of AC and Co–AC was calculated as 0.64 and 0.215 mLg^{-1} by the QS-DFT method.

The SEM images and EDS analysis show that Co–AC has channeled 3D porous structure and the structure contains carbon, nitrogen, oxygen, and cobalt elements homogenously distributed throughout Co–AC, as shown in Fig. 4. The cobalt and oxygen contents of 9.6% and 26%, respectively, show that the carbonized structure probably contains

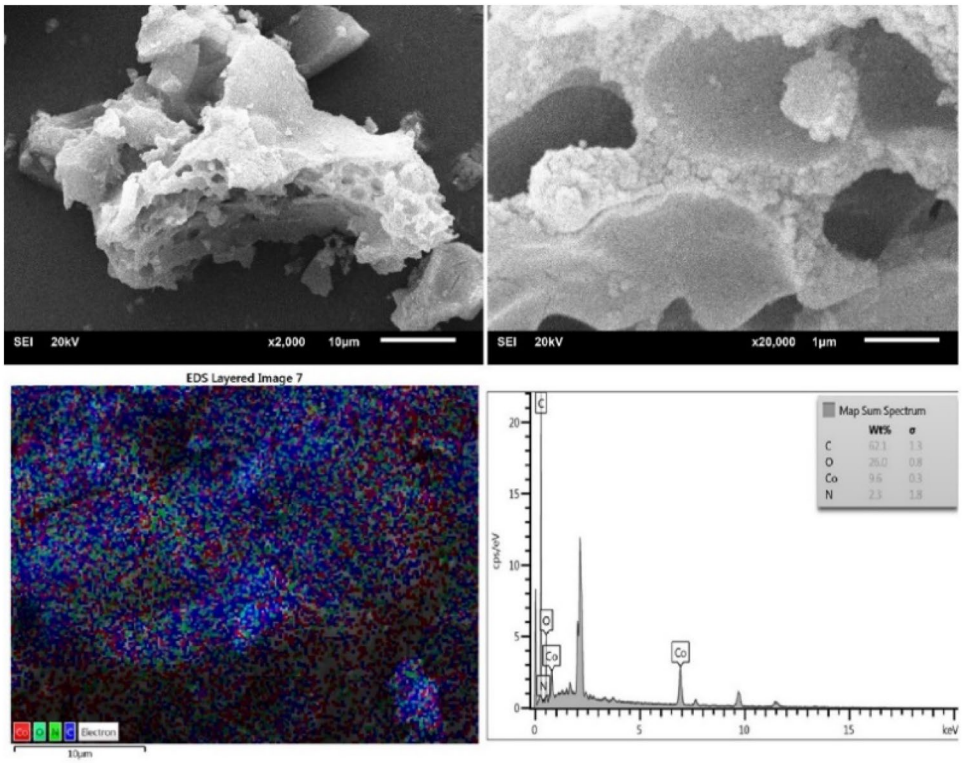

Fig. 4 SEM images, EDS map and elemental distribution of Co–AC

carbonyl oxygen except for oxygen of Co_3O_4. In addition, the presence of nitrogen element shows that nitrogen atoms were successfully doped on Co–AC.

The TEM images (Fig. 5) illustrate the nano-dot morphology of Co–AC. The dots with contrast show the presence of the Co_3O_4 and carbon structure [29]. As can be seen in

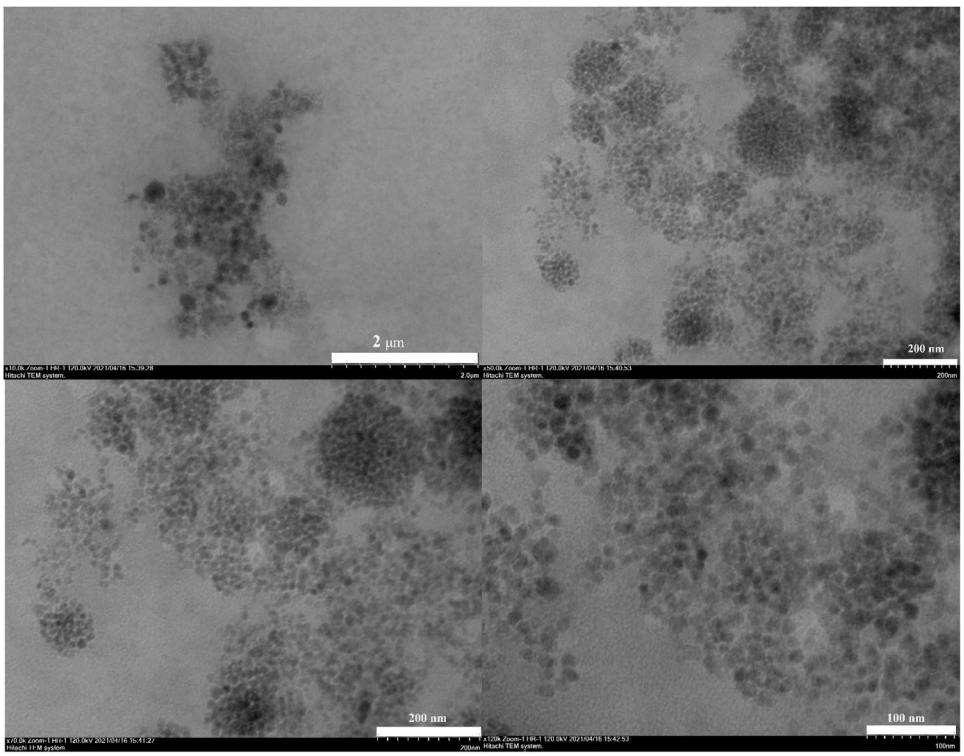

Fig. 5 TEM images of Co–AC

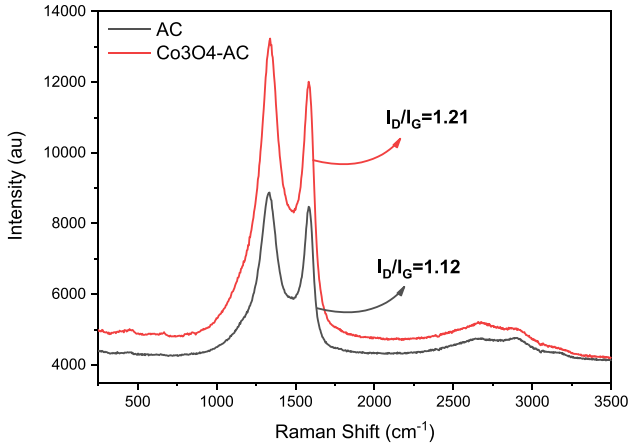

Fig. 6 Raman spectra of AC and Co–AC

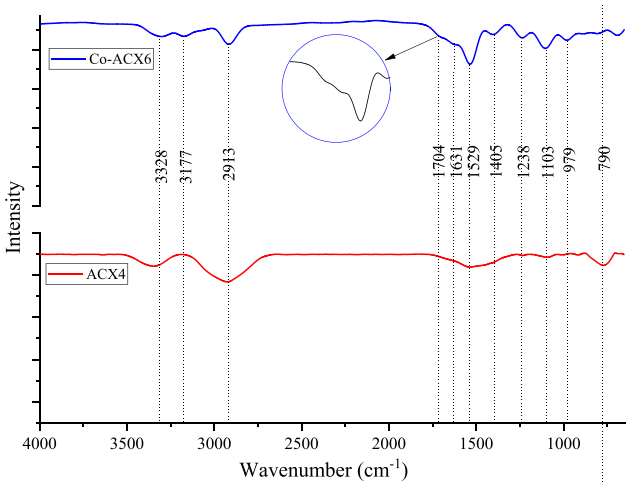

Fig. 7 IR spectrum of AC (red line) and Co–AC (blue line)

Fig. S3, the particle diameter of the Co_3O_4 nanostructures was about 13.65 ± 2.31 nm and the carbonized structure consisted of graphitic layered forms, confirmed by the carbon peaks of XRD and Raman spectra. The graphitization degree of activated carbon and Co–AC samples was investigated by Raman spectroscopy. As can be seen in Fig. 6, the bands caused by graphite (G) and defect disorder (D) were observed at about 1580 cm^{-1} and 1350 cm^{-1}, respectively. The ratio of the integrated intensities of these bands (I_D/I_G) is a measure of the graphitization and crystallinity of carbonaceous material. As a rule, while I_D/I_G ratio increases, crystallinity decreases and graphitization increases [30]. The I_D/I_G values of AC and Co–AC samples were calculated as 1.12 and 1.21. The increasing I_D/I_G value of Co–AC clearly shows that the doping of phthalocyanine cobalt complex on activated carbon caused an increase in the surface disorder degree. The increase in the surface disorder degree is due to partial degradation of the planar structure of phthalocyanines; especially, the isoindole moiety of phthalocyanine could be the main source of this disorder. While the planar form of the phthalocyanine ring supports the graphitization during the heating treatment, the degradation in the center of the phthalocyanine ring starting with the transformation of Co^{2+} to Co_3O_4 could increase the defect disorder.

FT-IR spectra of AC and Co–AC were recorded in the Perkin Elmer Spectrum One Spectrometer in the range of 4000–650 cm^{-1} as shown in Fig. 7. The samples were dried overnight in a vacuum oven to remove any adsorbed water before measurement. Both substances gave weak intensity and similar vibrational bands in their IR spectra. The broad vibration bands observed at 3228 cm^{-1} were interpreted as stretching vibrations from the OH groups that can be found in the structure. The broad bands observed at 2913 cm^{-1} are thought to belong to the aliphatic CH stretching vibrations belonging to the alkyl groups, and the weak vibrational bands observed at 1238 cm^{-1} and 1103 cm^{-1} are thought to belong to the stretching vibrations of C–O or C–N. The fact that these bands appear much more clearly in the FT-IR spectrum of Co–AC is because of the C–N bonds in the phthalocyanine molecule added to the structure. Vibration bands observed at 1704, 1631 and 1529 cm^{-1} in the IR spectrum of Co–AC indicate C=O, C=N, and C=C groups, respectively. These groups are most likely due to the carboxyl and imine groups formed during the degradation of the phthalocyanine molecule. Unlike the IR spectrum of AC, the weak band observed at 3177 cm^{-1} was interpreted as NH or OH stretching vibrations. The vibration band observed at 970 cm^{-1} was interpreted as C=C bending vibration. Two distinctive bands of Co–O stretching vibrations of Co_3O_4 observed at 663 and 576 cm^{-1} could not be observed, because they were not within the measuring range of the device.

Elemental analysis results confirm the presence of nitrogen in the structure. According to the results of elemental analysis, Co–AC contained 79.16% carbon, 7.26% nitrogen and 0.26% hydrogen (Fig. 8).

Table 2 illustrates the comparison of the catalytic activity of the Co–AC catalyst in RhB and 2,4,6-TCP solutions with previously reported systems of different catalysts and organic pollutants. It could be seen that Co-AC provides a high degradation yield, short reaction time and reusability compared to other catalysts and and degradation of other organic pollutants thought to be an efficient catalyst.

3.2 Effect of catalyst concentration

The effect of the concentration of Co–AC on catalytic performance was studied for catalytic degradation of RhB. The increase in catalyst concentration displayed a positive effect on catalytic degradation experiments in Fig. 9a. According to the results, about 75% degradation was achieved with 100 mL (12 mgL^{-1}) RhB dye solution, 75 mgL^{-1} catalyst

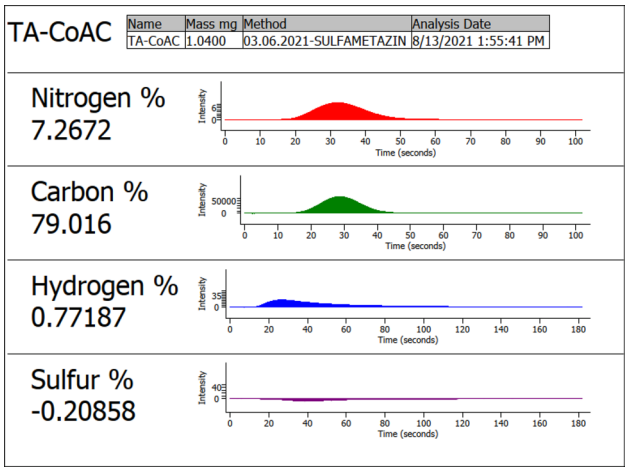

Fig. 8 Elemental analysis results of Co–AC

and 90 mgL^{-1} PMS at 25 °C at the end of the 16 min ($k = 0.0868\ min^{-1}$). After, the maximum degradation of RhB was observed when using 150 mgL^{-1} of catalyst. For 2,4,6-TCP, the increasing concentration of Co–AC displayed a positive effect on catalytic activity in degradation experiments. For instance, 94% degradation was obtained by using 5 mg Co–AC catalyst, 9 mg PMS and 25 mgL^{-1} 2,4,6-TCP 100 mL solution after 38 min ($k = 0.0740\ min^{-1}$). By increasing catalyst concentration to 15 mg, 100% degradation was achieved at the end of 6 min as shown in Fig. 10a.

As expected when catalyst concentration was increased, a greater number of active sites interacted to activate PMS. The increased activated sites could accelerate the reaction to generate more radicals for the degradation efficiency of RhB and 2,4,6-TCP.

3.3 Effect of PMS concentration

The radicals have an important role due to their high oxidation potentials for the degradation of pollutants. PMS is an important reagent due to its role in the production of radicals such as $SO4^{\cdot -}$ and $OH\cdot$ in the advanced oxidation process. This oxidant is activated by the catalyst and generates the radicals. Therefore, in addition to the type and concentration of catalysts, the concentration of PMS is highly important too and has a decisive effect on the course of the degradation reaction. The more radicals formed in the reaction medium, the faster and more efficient the catalytic decomposition can be expected. However, low catalyst concentration limits radical formation. In this regard, the effect of increasing the concentration of PMS on the degradation of RhB and 2,4,6-TCP is shown in Figs. 9b and 10b. PMS concentration was selected from 1.5 mg (0.024 mM) to 12 mg (0.196 mM) for RhB. The results showed that the maximum degradation was achieved by 9 mg PMS concentration ($k = 0.1676\ min^{-1}$) at the end of 16 min. When PMS concentration was increased to 12 mg, degradation reduced about 9% at the end of the

Table 2 Degradation of organic pollutants including different transition metal-based catalysts in the PMS system

Catalysts	Substrate	Reaction condition	Reaction time	References
Activated carbon	2,4,6-TCP	50 mgL^{-1} TCP, 0.75 gL^{-1} AC, 8 mM PMS, pH = 5	67.3% for 150 min	(2016), [49]
FePTS	2,4,6-TCP	0.1 mmol TCP solution, 5×10^{-4} mmol catalyst and 0.1 mmol PMS in 0.5 ml aqueous solution	74% for 30 min	(2017), [50]
$CoFe_2O_4$/GO	RhB	0,03 mM RhB, 0.1 mgL^{-1} PMS, 10 mg catalyst, T = 25 °C	98% for 12 min	(2018), [51]
CoAl-CLDH-300	RhB	10 mgL^{-1} RhB, 0.15 gL^{-1} catalyst, 0.5 mM PMS, T = 25 °C, pH = 5	99.6% for 30 min	(2019), [52]
α-MnO_2/Pal	RhB	20mgL^{-1} RhB, 0.10 gL^{-1} catalyst, 0.65 mM PMS, T = 25 °C, pH = 5.5	100% for 180 min	(2020), [53]
3%$FeCo_2O_4$/CN	RhB	20 mgL^{-1} RhB, 0.15 gL^{-1} PMS, 0.1 gL^{-1} catalyst and T = 25 °C	98% for 45 min	(2021), [54]
C@Cu-Ni	2,4,6-TCP	10 mgL^{-1} TCP, 0.1 gL^{-1} catalyst, 1 mM PMS, pH = 5	98.5% for 30 min	(2021), [55]
S@Fe-800	RhB	10 mgL^{-1} RhB, 0.2 gL^{-1} catalyst, 30 mM PMS	90% for 60 min	(2022), [56]
TiO_2-hemin	2,4,6-TCP	39.5 mgL^{-1} TCP, 20 mgL^{-1} catalyst, 150 mgL^{-1} PMS, pH = 5, T = 25 °C	92.9% for 10 min	(2022), [57]
Co − Fe/NC@GCS	Sulfamethoxazole	20 mgL^{-1} SFX, 200 mgL^{-1} catalyst, 0.5 mM PMS, pH = 5.76, T = 25 °C	93.8% for 60 min	(2022), [58]
CoCeTi	Phenanthrene	0.2 mgL^{-1} PAHs, 25 mgL^{-1} catalyst, 0.25 mM PMS, pH = 6.2, T = 25 °C	98.2% for 15 min	(2022), [59]
Co–RH-130	Carbamazepine	10 mgL^{-1} CBZ, 0.30 gL^{-1} catalyst, 0.30 gL^{-1} PMS,	95.7% for 60 min	(2022), [60]
FeCo-BC	Sulfamethoxazole	0.04 mM SFX, 100 mgL^{-1} catalyst, 0.4 mM PMS, pH = 3.4, T = 25 °C	100% for 10 min	(2022), [61]
Co–AC	RhB	12 mgL^{-1} RhB, 150 mgL^{-1} catalyst, 90 mgL^{-1} PMS, T = 25 °C	97.07% for 16 min	This work
	2,4,6-TCP	25 mgL^{-1} TCP, 150 mgL^{-1} catalyst, 90 mgL^{-1} PMS, T = 25 °C	100% for 6 min	This work

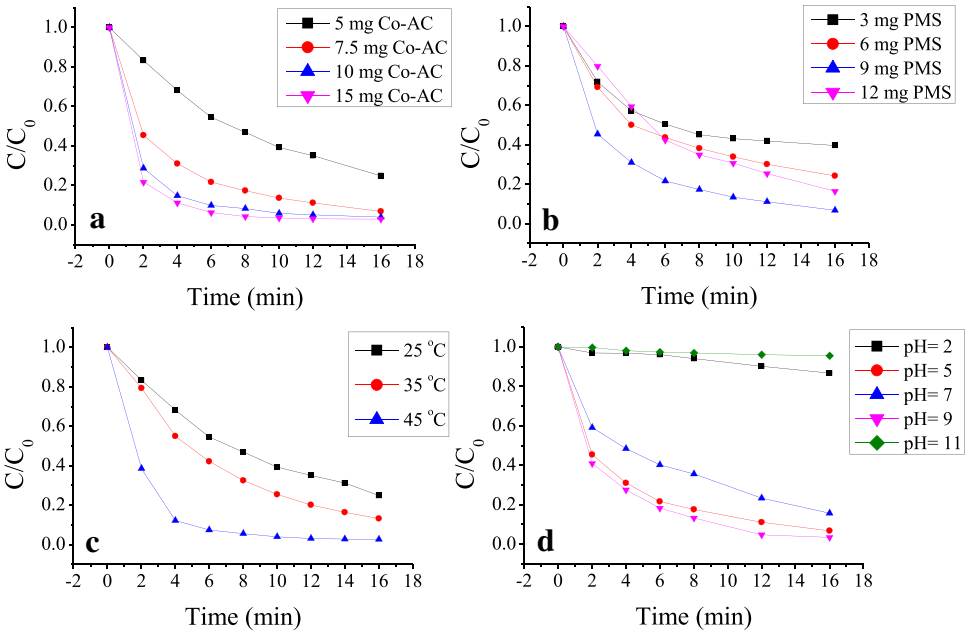

Fig. 9 **A** Effect of catalyst concentration on RhB degradation. Reaction conditions: [RhB] = 12 mgL^{-1}, [PMS] = 90 mgL^{-1}, temperature = 25 °C. **B** Effect of PMS concentration on RhB degradation. Reaction conditions: [RhB] = 12 mgL^{-1}, [catalyst] = 75 mgL^{-1}, temperature = 25 °C. **C** Effect of temperature on RhB degradation. Reaction conditions: [RhB] = 12 mgL^{-1}, [catalyst] = 50 mgL^{-1}, [PMS] = 90 mg/L. **D** Effect of pH on RhB degradation. Reaction conditions: [RhB] = 12 mgL^{-1}, [PMS] = 90 mgL^{-1}, [catalyst] = 75 mgL^{-1}, temperature = 25 °C

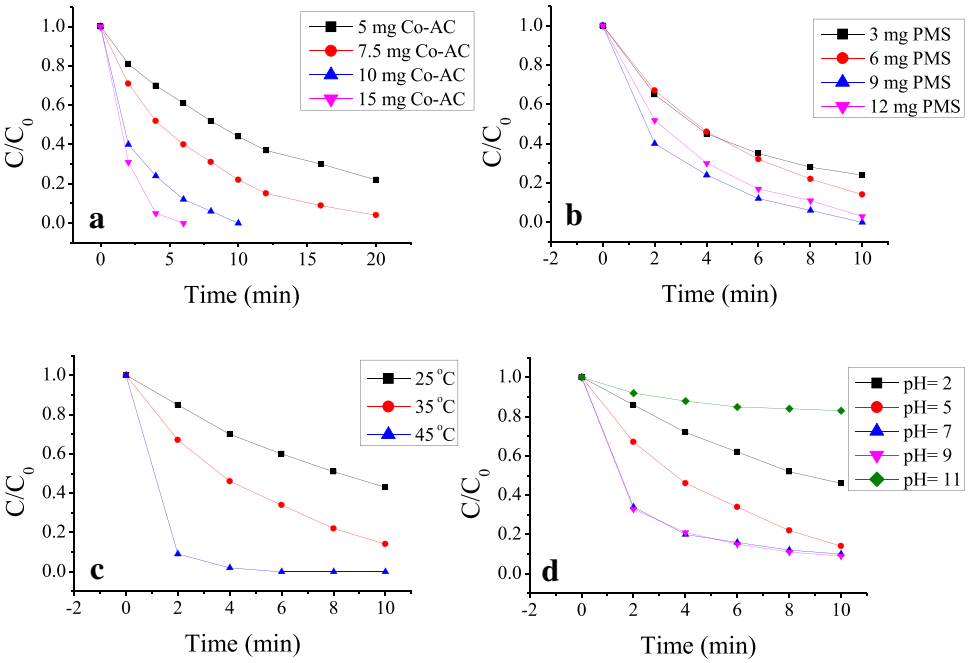

Fig. 10 **a** Effect of catalyst concentration on 2,4,6-TCP degradation. Reaction conditions: [2,4,6-TCP] = 25 mgL^{-1}, [PMS] = 90 mgL^{-1}, temperature = 25 °C. **b** Effect of PMS concentration on 2,4,6-TCP degradation. Reaction conditions: [2,4,6-TCP] = 25 mgL^{-1}, [catalyst] = 100 mgL^{-1}, temperature = 25 °C. **c** Effect of temperature on 2,4,6-TCP degradation. Reaction conditions: [2,4,6-TCP] = 25 mgL^{-1}, [catalyst] = 100 mgL^{-1}, [PMS] = 60 mgL^{-1}. **d** Effect of pH on 2,4,6-TCP degradation. Reaction conditions: [2,4,6-TCP] = 25 mgL^{-1}, [catalyst] = 100 mgL^{-1}, [PMS] = 60 mgL^{-1}, temperature = 25 °C

16th min ($k = 0.1125\ min^{-1}$). This reduction can be due to high PMS concentration acting as a scavenger for sulfate radical [31]. According to these results, the maximum amount of radical production was limited by fixed catalyst concentration. At a low concentration of PMS, color removal efficiency and rate constant significantly diminished, but at the highest concentration of PMS, catalytic activity slightly decreased.

3.4 Effect of temperature on degradation of RhB

To investigate the effect of temperature on the degradation of RhB and 2,4,6-TCP, the reactions were implemented at different temperatures as shown in Fig. 9c and 10c. It was observed that almost all of the RhB was degraded when the temperature increased from 25 °C to 45 °C, in a much shorter time than that of reactions at a lower temperature, when the other conditions were held constant (Co–AC (75

mgL^{-1})/PMS (90 mgL^{-1})). Compared to the degradations at 25 °C, 35 °C and 45 °C temperatures in 10 min, 75.07% ($k = 0.0868\ min^{-1}$), 86.77% ($k = 0.1264\ min^{-1}$) and 97.38% ($k = 0.2276\ min^{-1}$) yields were obtained, respectively.

For 2,4,6-TCP, the temperature was increased from 25 °C to 45 and catalytic degradation accelerated and 100% degradation was obtained at 45 °C. With rise in temperature, $k = 0.0891\ min^{-1}$ for 25 °C, $k = 0.1941\ min^{-1}$ for 35 °C and $k = 0.9780\ min^{-1}$ for 45 °C reaction rate constants were achieved in 4 min. The results showed that catalytic activity increased with raising the temperature for both the contaminants.

3.5 Effect of pH

The effect of the initial pH values of RhB and 2,4,6-TCP aqueous solutions on degradation efficiency were investigated from 2 to 11 for RhB and 2,4,6-TCP throughout a 16 min period of the reaction time as shown in Figs. 9d and 10d. On comparison of the acidic and basic conditions, it was seen that the catalyst was more suitable and efficient at pH values 5–9 for the catalytic degradation of RhB. When the pH value was increased from 9 to 11 or decreased from 5 to 2, the degradation efficiency decreased from 96.4 to 4.4% or from 93.2% to 13.22%. The obtained results showed that this decline in degradation may result in PMS due to self-decomposition with a non-radical route [32] because H^+ ions can quench $SO_4^{\cdot -}$ and OH· radicals at very low pH 2 values as shown in Eqs. (2) and (3). Moreover, the form of PMS in the current solution were defined by dye solution pH, such as HSO_5^-, the main species in acidic and neutral pH values [33].

When the effect of pH on degradation of 2,4,6-TCP was examined, the catalyst worked effectively in the range of pH 5 and 9 with 86% ($k = 0.1966\ min^{-1}$) and 91% ($k = 0.2407\ min^{-1}$) yields for 10 min. The degradation yield diminished to 54% and 17% at pH 3 and 11, respectively. These decreases in degradation occurred due to the above-mentioned reasons.

$$\cdot OH + H^+ + e^- \rightarrow H_2O, \tag{3}$$

$$SO_4^{\cdot -} + H^+ + e^- \rightarrow HSO_4^{\cdot -}. \tag{4}$$

3.6 Radical and non-radical quenching experiments

In general, activated PMS by transition metal oxides could produce $SO_4^{\cdot -}$, OH· and $SO_5^{\cdot -}$radicals [34]. $SO_4^{\cdot -}$ and OH· radicals are major active species between these radicals for catalytic degradation of organic pollutants. Ethanol (EtOH) is usually used as a scavenger for quenching $SO_4^{\cdot -}$ and OH· radicals due to their high reaction rate constants $k = 1.2 \times 10^9$–$2.8 \times 10^9\ M^{-1}\ s^{-1}$ for OH· and 1.6×10^7–$7.7 \times 10^7\ M^{-1}\ s^{-1}$ for $SO_4^{\cdot -}$, and *tert*-butyl alcohol (TBA) was chosen only as scavenger OH·radicals because its reaction rate constant for OH· ($k = 3.8 \times 10^8$–$7.6 \times 10^8\ M^{-1}\ s^{-1}$) was significantly higher than that for $SO_4^{\cdot -}$ ($k = 4 \times 10^5$–$9.1 \times 10^5\ M^{-1}\ s^{-1}$) [35]. In this regard, we studied with 50 mM TBA and EtOH, scavenger/PMS (5000:1) ratio, as a scavenger to determine major reactive radical species in the Co–AC/PMS system for quenching experiments. As shown in Fig. 11a, catalytic degradation of RhB without any radical scavenger no scavenger was 93.18%

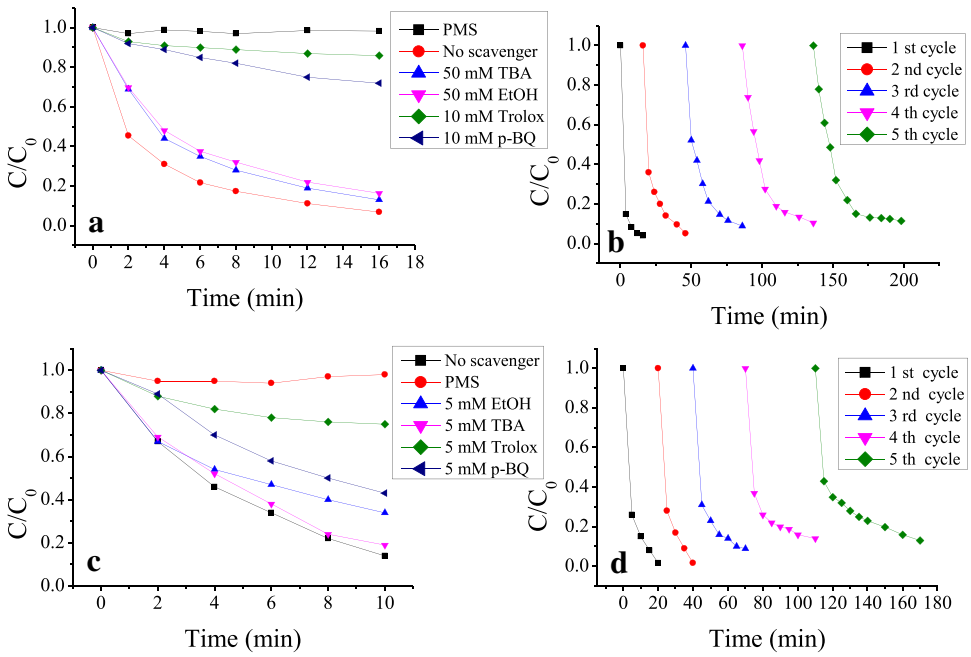

Fig. 11 **a** Radical quenching experiments of RhB. Reaction conditions: [RhB] = 12 mgL^{-1}, [catalyst] = 75 mgL^{-1}, [PMS] = 90 mgL^{-1}, temperature = 25 °C. **b** Experiment of reusability of catalyst on RhB degradation. Reaction conditions: [RhB] = 12 mgL^{-1}, [catalyst] = 100 mgL^{-1}, [PMS] = 90 mgL^{-1}, temperature = 25 °C. **c** Radical quenching experiments of 2,4,6-TCP degradation. Reaction conditions: [2,4,6-TCP] = 25 mgL^{-1}, [catalyst] = 100 mgL^{-1}, [PMS] = 60 mgL^{-1}, temperature = 25 °C. **d** Experiment of reusability of catalyst on 2,4,6-TCP degradation. Reaction conditions: [2,4,6-TCP] = 25 mgL^{-1}, [catalyst] = 100 mgL^{-1}, [PMS] = 60 mgL^{-1}, temperature = 25 °C

(k=0.1678 min^{-1}) for 16 min. However, catalytic degradation was decreased from 93.18% to 87% and 83.7% in the presence of TBA and EtOH, respectively. The reaction rate constants were 0.1132 min^{-1} for EtOH and 0.1275 min^{-1} for TBA. As compared to catalytic degradation efficiency with EtOH and TBA, further degradation in the presence of TBA was seen and $SO_4^{\cdot -}$ radical was more dominant than OH· radical in the Co–AC/PMS system. In addition, we observed degradation of RhB significantly reduced with the addition of *p*-BQ as $O_2^{\cdot -}$ quencher (k=0.0205 min^{-1}) and Trolox as $^1O_2$ quencher (k=0.0094 min^{-1}). According to these reaction rate constants, $^1O_2$ radical was superior to other radical species in the quenching experiments.

For 2,4,6-TCP, radical quenching experiments were applied with a similar procedure with RhB as shown in Fig. 11c. The reaction rate constant values were 0.1078 min^{-1} for EtOH, 0.1660 min^{-1} for TBA, 0.0843 min^{-1} for *p*-BQ and 0.0287 min^{-1} for Trolox. In line with the obtained results, degradation of 2,4,6-TCP decreased from 86 to 25% with the addition of Trolox. In this way, $^1O_2$ radical was more effective than other radicals for degradation. The Co–AC/PMS system displayed both radical ($SO_4^{\cdot -}$, OH·, $O_2^{\cdot -}$) and non-radical ($^1O_2$) pathways according to the obtained experimental data. We proposed the possible non-radical pathway for degradation of RhB and 2,4,6-TCP as shown in Fig. 12.

As reported, transition metal ions such as Co(II) can activate PMS to generate sulfate radicals as follows (Eqs. (4)–(11)) [36–38].

$$Co^{2+} + H_2O \leftrightarrow CoOH^+ + H^+, \quad (4)$$

$$Co^{2+} + HSO_5^- \rightarrow Co^{3+} + SO_4^{\cdot -} + H_2O \quad (5)$$

$$CoOH^+ + HSO_5^- \rightarrow CoO^+ + SO_4^{\cdot -} + H_2O, \quad (6)$$

$$CoO^+ + 2H^+ \rightarrow Co^{3+} + H_2O, \quad (7)$$

$$Co^{2+} + SO_4^{\cdot -} \rightarrow Co^{3+} + SHO_4^{2-}, \quad (8)$$

$$Co^{2+} + \cdot OH^+ \rightarrow Co^{3+} + OH^-, \quad (9)$$

$$Co^{3+} + HSO_2^- \rightarrow Co^{2+} + SO_5^{\cdot -} + H^+, \quad (10)$$

$$HSO_5^- + SO_5^{2-} \rightarrow SHO_4^- + SHO_4^{2-} + {}^1O_2, \quad (11)$$

$$\text{RhB} + \text{2,4,6-TCP} + {}^1O_2 \rightarrow \text{Degradation products} + CO_2 + H_2O. \quad (12)$$

3.7 The stability and reusability of the Co–AC catalyst

The stability of the Co–AC catalyst (100 mgL^{-1}) was investigated with a reusability experiment of the degradation of RhB (12 mgL^{-1}) in the presence of PMS (90 mgL^{-1}) as shown in Fig. 11b. When each cycle ended, a fresh concentrated solution of RhB to obtain the initial concentration of RhB and 6 mg PMS was added to the reaction media. Five cycles were studied for stability and 96.03% degradation was seen at the end of the first cycle for 16 min. Then, 93.11, 91.06, 89.49 and 88.5% degradation efficiency was obtained at the end of five cycles, respectively. As a result of this study, the Co–AC catalyst exhibited good stability and efficiency with 88.5% degradation at end of the five cycles after 62 min.

For the stability and reusability of Co–AC in 25 mgL^{-1} of 2,4,6-TCP solution, 100 mgL^{-1} catalysts and 60 mgL^{-1} PMS were chosen for the first cycle and obtained 98.3% degradation after 20 min. Then, for the other cycle, the fresh

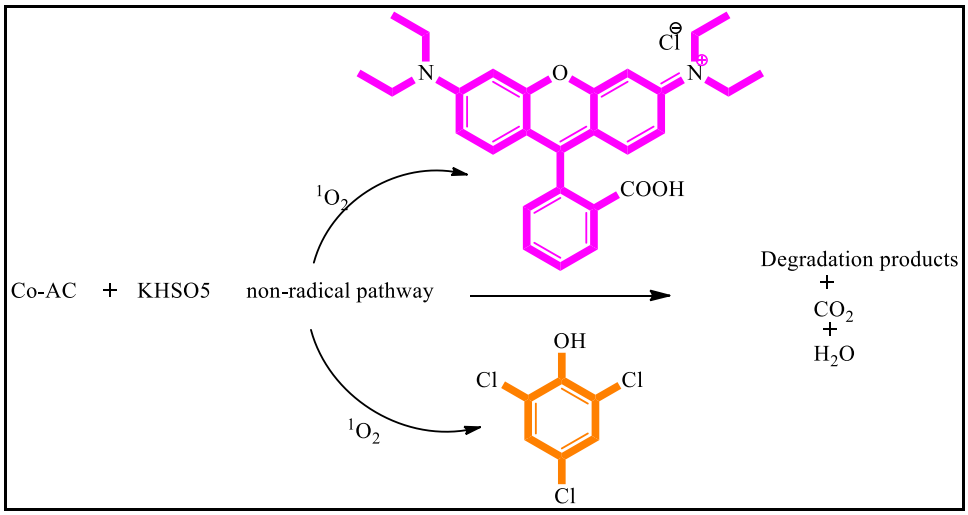

Fig. 12 The possible non-radical pathway for catalytic degradation of RhB and 2,4,6-TCP

concentrated 2,4,6-TCP solution was poured into the reaction media and 6 mg PMS was added as in the above procedure of RhB. At the end of the five cycles, 87% degradation was achieved in 60 min as shown in Fig. 11d. This Co–AC catalyst displayed nearly the same stability and efficiency for both RhB and 2,4,6-TCP contaminants.

3.8 TOC and ICP-OES analysis

To investigate the mineralization degree of RhB and 2,4,6-TCP, total organic carbon (TOC) removal efficiency of Co–AC/PMS was tested in the catalytic oxidation process. TOC analysis was performed by Shimadzu TOC-L analyzer (Japan). It is clear from the obtained results that TOC removal % was 46 for RhB, while it was 66 for 2,4,6-TCP at the end of the reactions as shown in Fig. 13. Comparison of the TOC removal value of RhB with that of 2,4,6-TCP ahowed that the lower TOC removal may be due to the resistance of the aromatic RhB oxidation products [39].

Transition metal leaching is an important issue in heterogeneous catalyst systems, as it is a potential threat to the environment. Moreover, cobalt is known to be a superior activator for PMS, and high cobalt leaching shows a negative effect on the degradation of organic wastes as catalyst performance decreases [40]. Therefore, the cobalt leaching tests were separately performed for RhB and 2,4,6-TCP. The solutions obtained at the end of the reactions were diluted to certain amounts and analyzed with ICP-OES OPTİMA 7000 DV (Perkin Elmer, USA). According to the results, the leaching values of cobalt were 1.35 mgL^{-1} and 1.38 mgL^{-1} for RHB and 2,4,6-TCP as shown in Fig. 13. This study is

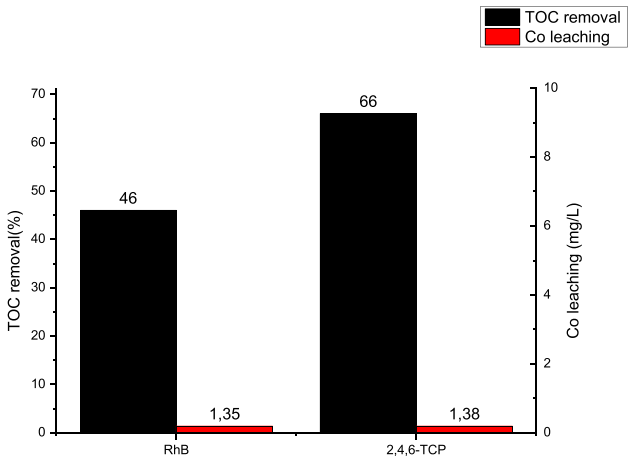

Fig. 13 TOC and Co leaching values of RhB and 2,4,6- TCP at the end of reaction (reaction conditions for TOC and ICP-OES analysis: [catalyst] = 100 mgL^{-1}, [RhB] = 12 mgL^{-1}, [PMS] = 90 $mgL^{-1}$and temperature = 25 °C for RhB/Co–AC system and [catalyst] = 100 mgL^{-1}, [2,4,6-TCP] = 25 mgL^{-1}, [PMS] = 90 $mgL^{-1}$and temperature = 25 °C for 2,4,6-TCP /Co–AC system also no pH adjustment for RhB and 2,4,6-TCP)

acceptable when these values of cobalt leaching were compared to previous works such as 1.669 mgL^{-1} for $MnCo_2O_{4.5}$ [41], 9 mgL^{-1} for Co-BTC(A) [42], 63.18 mgL^{-1} for activated carbon(AC)-supported Co_3O_4-based catalyst [43], 1.82 mgL^{-1} for Co–SMA [44], 1 mgL^{-1} for BC–Co_3O_4 [45], 0.9 mgL^{-1} for $CoFeO_2$@CN, 1.4 mgL^{-1} for pristine $CoFeO_2$ [46], 3.23 mgL^{-1} for commercial Co_3O_4 [47] and 3 mgL^{-1} for Co_1Fe_1-300 [48], in the literature.

3.9 Comparison with other studies

Table 2 compares the degradation of rhodamine B, 2,4,6-trichlorophenol and other organic pollutants using different temperature, pH, catalyst and PMS concentrations. According to the results, the degradation efficiency for the synthesized Co–AC is excellent when compared with activated carbon, iron porphyrine tetrasulfonate, cobalt magnetite graphene oxide, cobalt aluminum composite, alpha manganese oxide/palygorskite, iron cobaltite carbon nitride, copper–nickel hybrid material, cobaltite-loded biochar and biomass and TiO_2–hemin catalysts.

Ghanbari et al. [49] investigated the degradation of 2,4,6-trichlorophenol under UV light with peroxymonosulfate activation and activated carbon. According to the optimization parameters, approximately 67% degradation occurred in 150 min in the presence of pH: 5, 8 mM PMS and 750 mg/L catalyst. In addition, better performance was obtained in acidic conditions and the sulfate radical played an important role in the degradation experiment. The degradation efficiency and time obtained in this study are very high compared to Co–AC. In addition, the amount of PMS used is 13 times more.

Çimen et al. [50] studied the degradation of 2,4,6-trichlorophenol in a methanol–water mixture in the presence of iron porphyrin tetrasulfonate/PMS. 74% degradation was obtained in 30 min under conditions of 0.1 mmol TCP solution, 5 × 10–4 mmol catalyst and 0.1 mmol PMS in 0.5 ml aqueous solution. It was observed that the activity of the catalyst decreased after the first cycle. This limits the reusability of the catalyst. When this study is compared with Co–AC, the degradation efficiency is very low and also the reusability of the catalyst is significantly reduced after the first cycle.

Tabit et al. [51] doped magnetite cobalt ferrite on the graphene oxide surface and studied the rhodamine B degradation. In the study, they found that CoFe2o4/GO catalyst had more effective catalytic activity than cobalt ferrite and different temperature, pH, catalyst and PMS concentrations were studied. Due to the magnetite feature of the catalyst, it is easily separated from the aqueous environment with an external magnet. They obtained a catalyst with high stability and reusability.

For the treatment of water contaminated with organic pollutants, Zhu et al. [52] synthesized CoAl-layered double hydroxide (CoAl-LDH) and calcined (CoAl-CLDH) highly active, stable heterogeneous catalysts that could be studied in a wide pH range.The experiments showed that the separation of metal ions from the catalyst could be significantly reduced by calcination. It was revealed that singlet oxygen ($^1O_2$) was dominant in the catalytic degradation of stable CoAl-CLDH and rhodamine B in the presence of PMS for 30 min 99.6% degradation. When these results are compared with the presented study, the degradation time of rhodamine B for CoAl-CLDH is longer than that of Co–AC, although the catalyst is active over a wide pH range.

Huang et al. [53] fabricated nanorod α-MnO2 loaded with large surface area crystalline mineral palygorskite (α-MnO2/Pal) by a simple hydrothermal method. α-MnO2/Pal was used to activate PMS for RhB degradation. Nearly 100% RhB degradation was obtained in the α-MnO2/Pal and PMS system in 180 min, and the RhB degradation efficiency increased with increasing α-MnO2/Pal doses, PMS doses and temperatures. Degradation was inhibited at pH > 5.5, but increased at pH < 5.5. The main reactive radicals responsible for RhB degradation classified by the radical quenching test were O^{2-} and $^1O_2$. Compared to Co–AC, although the degradation efficiency was very high in this study, the degradation time was very long. It also shows activity in a very narrow pH range.

$FeCo_2O_4$ has been widely investigated because of its stable structure and environmental properties. Zhao et al. [54] synthesized composites of graphite carbon nitride (g-C3N4) and spinel iron cobaltate ($FeCo_2O_4$) for degradation of rhodamine B by combining photocatalytic and Fenton-like reactions. The composite containing 3%FeCo2O4/CN showed the best degradation efficiency, with approximately 98% RhB degraded in 45 min. While the decomposition time was prolonged only in g-C3N4, the decomposition time was shortened with the addition of $FeCo_2O_4$. However, decomposition occurs more slowly with the addition of 5% $FeCo_2O_4$.

In another study, Zhang et al. [55] designed (C@CueNi) by embedding magnetic Cu and Ni bimetallic particles to carbon sheets with calcination of a mixture of Cu-MOF and Ni-MOF (mass ratio = 4:6) under N_2 atmosphere and used as a catalyst for degradation of 2,4,6-TCP. The results showed that more than 98.5% of 2,4,6-TCP (10 mg L^{-1}) dissociated rapidly within 30 min at initial pH = 5, PMS = 1 mM and catalyst dose = 0.1 g L^{-1}. This excellent catalytic activity was derived from the synergistic effect of carbon, copper and nickel. Another feature of this catalyst is that it is easily separated from the aqueous environment due to its magnetite structure and its reusability is high. Compared with the Co–AC/PMS system, the degradation time and PMS concentration are high, although the 2,4,6-TCP concentration is low.

Yu et al. [56] used anaerobic granular sludge for biochar production due to its individual microstructure and high organic content to synthesize Fe_3O_4-loaded biochar as a catalyst for peroxymonosulfate activation. This catalyst was optimized by iron modification at different temperatures. This biochar was calcined at 800 °C and displayed a larger specific surface area, richer porous structures and greater Fe_3O_4 content. The excellent magnetic properties of the iron-modified biochar at 800 °C (S@Fe-800) were confirmed. S@Fe-800 exhibited outstanding PMS activation ability for removal efficiency of rhodamine B. Although the catalyst and PMS concentration was higher than that of the Co–AC/PMS system, the degradation time was high and the degradation efficiency was low.

The PMS activation with metalloporphyrin loaded on TiO_2 has not been investigated. Chen et al. [57] prepared TiO_2–hemin catalyst by immobilizing hemin on TiO2 using the ball-milling method. Compared with the hemin and TiO_2, the synthesized TiO_2–hemin demonstrated highly catalytic degradation of 2,4,6-TCP. The catalytic degradation efficiency observed in the PMS activation system was high and 92.9% of the 2,4,6-Trichlorophenol was removed within 10 min. The excellent performance is based on the strong interaction between TiO_2 and hemin due to electron density of the hemin structure.

Zhao et al. [58] constructed a micro-nano-reactor, in which MOF-derived Co–Fe nitrogen-doped graphitic carbon nanocatalysts are covered in a glutaraldehyde–cross-linked chitosan microsphere to activate PMS for degradation of sulfamethoxazole. This catalyst, which was synthesized to reduce metal ion release and activate PMS, showed a degradation efficiency of 93.8% in 60 min. At the same time, they stated that this material would be effective in the degradation of other organic pollutants by activating PMS as an adsorbent or catalyst.

Wang et al. synthesized low concentration of Co and Ce with CoCeTi by a facile one-step sol–gel solvotermal method [59]. Porous broken sponge-like structures were observed in catalyst morphology. Phenanthrene degradation rate was 98.2% in 15 min and 100% degradation was achieved in 60 min (in pH = 3–9). $SO_4^{\cdot -}$, $O_2^{\cdot -}$, $^1O_2$ and h^+ were confirmed as dominant reactive species for degradation. This catalyst can be used to degrade other phenolic pollutants because of the stability, preparation and good activation of PMS, but its reusability was reduced about 80% in the third cycle.

Zhai et al. converted rice hulls into catalytic material by the combustion method and cobalt was doped by hydrothermal carbonization [60]. Low cost and environmentally friendly cobalt-doped hydrochar catalyst exhibited excellet degradation, due to the active sites of the catalyst for carbamazepine of 95.78% in 60 min by efficiently activating PMS. The reusability tests showed high stability and recyclability

due to the synergy of biochar and cobalt oxide. In radical species identification experiments, sulfate and peroxide radicals were dominant.

Wang et al. [61] prepared a single metal and bimetallic catalyst doped into biochar. Iron- and cobalt-doped biochar showed more catalytic activity than only iron- and copper-doped biochar catalysts. Within 10 min, all of the sulfamethoxazole was degraded. This study leads to the preparation of removal of recalcitrant organic pollutants of biochar-supported bimetallic catalysts with high efficiency and stability.

Compared to other catalysts, there was high efficiency of Co–AC based on increasing the electron transfer of the nitrogen atoms in the structure and abundance of active sites on the catalyst surface due to the morphology of carbon and nitrogen, as well as being a good activator for PMS of cobalt doped into the activated carbon support material. Thus, by accelerating the formation of reactive oxygen species, organic pollutants on the activated carbon surface react effectively with the catalyst and undergo oxidation. The synthesized material can be a good catalyst for other organic pollutants in wastewater treatment.

4 Conclusion

Cobalt phthalocyanine was used as the metal and nitrogen source, while the activated carbon was selected as the solid support used for the first time in this study. The phthalocyanine Co(II) complex was impregnated in commercial activated carbon and the product was carbonized at 800 °C. N_2 adsorption studies showed that phthalocyanine Co(II) was located on micropores smaller than 2 nm. It was confirmed by analysis of FT-IR, elemental, SEM, XRD, TEM and Raman spectroscopy that Co–AC also consists of graphite-like layered structures and contains nitrogen atoms. The catalytic degradation system was set on Co–AC, PMS and RhB and 2,4,6-TCP. Within the scope of the catalytic study, the effect of PMS concentration, reaction temperature, the concentration of catalyst, the pH of the solution on the reaction rate and recycling performance was investigated and optimal conditions were determined. 97% degradation value was observed in 16 min at 25 °C, but no pH adjustment. In addition, 97.38% degradation was reached by increasing temperature up to 45 °C in 10 min and optimum pH value was obtained at 9, but degradation decreased to 4.4% at pH 11. At the end of five cycles, 88.5% stability was observed in the RhB/PMS system. For 2,4,6-TCP, 100% degradation was seen in 6 min at 45 °C without applying pH. The degradation efficiency was diminished to 17% by high pH. It is found that Co–AC is more effective in a shorter time for 2,4,6-TCP in this study. Comparing results of this study with that previously reported, it can be said that the Co–AC may be the model catalyst for both degradations of RhB and 2,4,6-TCP. Although Co–AC is easily prepared and has a high effective decomposition efficiency, it shows activity in a narrow pH range such as pH 5–9. To eliminate this disadvantage, solid support material can be changed or bimetallic forms can be doped into activated carbon. In further studies, the catalytic activity of Co–AC will be investigated thanks to its high reaction yield, short reaction time and moderate recycling performance.

Supplementary Information The online version contains supplementary material available at https://doi.org/10.1007/s42823-022-00452-5.

Declarations

Conflict of interest There are no potential conflicts of interest relevant to this article.

References

1. Pearce CI, Lloyd JR, Guthrie JT (2003) The removal of colour from textile wastewater using whole bacterial cells: a review. Dye Pigment 58:179–196
2. Roberts ALK, Fletcher JM, Moore L, Byers S (2010) Trans-generational exposure to low levels of rhodamine B does not adversely affect litter size or liver function in murine mucopolysaccharidosis type IIIA. Mol Genet Metab 101:208–213. https://doi.org/10.1016/j.ymgme.2010.06.008
3. Dai Z, Ren PG, Zhang H et al (2021) Nitrogen-doped and hierarchically porous carbon derived from spent coffee ground for efficient adsorption of organic dyes. Carbon Lett 31:1249–1260. https://doi.org/10.1007/s42823-021-00248-z
4. Jin T, Liu C, Chen F et al (2022) Synthesis of g-C3N4/CQDs composite and its photocatalytic degradation property for Rhodamine B. Carbon Lett 32:1451–1462. https://doi.org/10.1007/s42823-022-00382-2
5. Li H, Kuang X, Shen X, Zhu J (2020) Comparative electrochemical oxidation of the secondary effluent of petrochemical wastewater with electro-fenton and anodic oxidation with supporting electrolytes. Environ Technol (United Kingdom) 43:1–24. https://doi.org/10.1080/09593330.2020.1791971
6. Rakhmania A, Kamyab H, Yuzir MA et al (2022) Electrochemical oxidation of palm oil mill effluent using platinum as anode: optimization using response surface methodology. Environ Res 214:113993. https://doi.org/10.1016/j.envres.2022.113993
7. Hazarika KK, Hazarika D, Bharali P (2020) Binary α-Fe2O3–Co3O4 nanostructures for advanced oxidation process: role of synergy for enhanced catalysis. Appl Organomet Chem 34:1–11. https://doi.org/10.1002/aoc.5920
8. Qin FX, Jia SY, Liu Y et al (2013) Metal-organic framework as a template for synthesis of magnetic CoFe 2O4 nanocomposites for phenol degradation. Mater Lett 101:93–95. https://doi.org/10.1016/j.matlet.2013.03.085
9. Jiang Y, Wan S, Zhao W et al (2022) Reusable, magnetic laser-induced graphene for efficient removal of organic pollutants from water. Carbon Lett 32:1047–1064. https://doi.org/10.1007/s42823-022-00336-8
10. Yang S, Li L, Xiao T et al (2017) Reuse performance of granular-activated carbon and activated carbon fiber in catalyzed peroxymonosulfate oxidation. Environ Technol (United Kingdom) 38:598–605. https://doi.org/10.1080/09593330.2016.1205147
11. Sudhaik A, Raizada P, Thakur S et al (2020) Metal-free photoactivation of peroxymonosulfate using graphene supported

graphitic carbon nitride for enhancing photocatalytic activity. Mater Lett 277:128277. https://doi.org/10.1016/j.matlet.2020.128277
12. Ramesh M, Rajeshkumar L, Bhoopathi R (2021) Carbon substrates: a review on fabrication, properties and applications. Carbon Lett 31:557–580. https://doi.org/10.1007/s42823-021-00264-z
13. Du J, Xu W, Liu J, Zhao Z (2020) Efficient degradation of Acid Orange 7 by persulfate activated with a novel developed carbon-based MnFe2O4 composite catalyst. J Chem Technol Biotechnol 95:1135–1145. https://doi.org/10.1002/jctb.6298
14. Ren Z, Romar H, Varila T et al (2021) Ibuprofen degradation using a Co-doped carbon matrix derived from peat as a peroxymonosulphate activator. Environ Res 193:110564. https://doi.org/10.1016/j.envres.2020.110564
15. Xu H, Zhang Y, Li J et al (2020) Heterogeneous activation of peroxymonosulfate by a biochar-supported Co3O4 composite for efficient degradation of chloramphenicols. Environ Pollut 257:113610. https://doi.org/10.1016/j.envpol.2019.113610
16. Zhao DY, Wang HL, Qi HP, Zhao Y (2019) Facile synthesis of mesoporous Co3O4 with excellent performance for activation of PMS. Mater Res Express. https://doi.org/10.1088/2053-1591/ab1686
17. Zeng T, Zhang H, He Z et al (2016) Mussel-inspired approach to constructing robust cobalt-embedded N-doped carbon nanosheet toward enhanced sulphate radical-based oxidation. Sci Rep 6:2–10. https://doi.org/10.1038/srep33348
18. Hu Y, Chen D, Wang S et al (2022) Activation of peroxymonosulfate by nitrogen-doped porous carbon for efficient degradation of organic pollutants in water: performance and mechanism. Sep Purif Technol. https://doi.org/10.1016/j.seppur.2021.119791
19. Kwiatkowski M, Broniek E (2020) An evaluation of the reliability of the results obtained by the LBET, QSDFT, BET, and DR methods for the analysis of the porous structure of activated carbons. Materials (Basel). https://doi.org/10.3390/MA13183929
20. Ghani F, Kristen J, Riegler H (2012) Solubility properties of unsubstituted metal phthalocyanines in different types of solvents. J Chem Eng Data 57:439–449. https://doi.org/10.1021/je2010215
21. Sundar M, Easwaramoorthy D, Kutti Rani S, Mohammed Bilal I (2008) Mn(II) catalysed decomposition of peroxomonosulphate—Kinetic and mechanistic study. Catal Commun 9:2340–2344. https://doi.org/10.1016/j.catcom.2008.05.024
22. Rasalingam S, Wu CM, Koodali RT (2015) Modulation of pore sizes of titanium dioxide photocatalysts by a facile template free hydrothermal synthesis method: Implications for photocatalytic degradation of rhodamine B. ACS Appl Mater Interfaces 7:4368–4380. https://doi.org/10.1021/am508883f
23. Bisbyb RH, Morgan CG, Hamblett I, Gorman AA (1999) Quenching of Singlet Oxygen by Trolox C, Ascorbate, and Amino Acids: Effects of pH and Temperature. J Phys Chem A 103:7454–7459. https://doi.org/10.1021/jp990838c
24. Khan A, Zou S, Wang T et al (2018) Facile synthesis of yolk shell Mn2O3@Mn5O8 as an effective catalyst for peroxymonosulfate activation. Phys Chem Chem Phys 20:13909–13919. https://doi.org/10.1039/c8cp02080a
25. Qin Q, Gao X, Wu X, Liu Y (2019) NaBH4-treated cobalt-doped g-C3N4 for enhanced activation of peroxymonosulfate. Mater Lett 256:126623. https://doi.org/10.1016/j.matlet.2019.126623
26. Kang M, Zhou H (2015) Facile synthesis and structural characterization of Co3O4 nanocubes. AIMS Mater Sci 2:16–27. https://doi.org/10.3934/matersci.2015.1.16
27. Üner O, Bayrak Y (2018) The effect of carbonization temperature, carbonization time and impregnation ratio on the properties of activated carbon produced from Arundo donax. Microporous Mesoporous Mater 268:225–234. https://doi.org/10.1016/j.micromeso.2018.04.037
28. Kumar A, Jena HM (2016) Preparation and characterization of high surface area activated carbon from Fox nut (Euryale ferox) shell by chemical activation with H3PO4. Results Phys 6:651–658. https://doi.org/10.1016/j.rinp.2016.09.012
29. Aluha J, Abatzoglou N, Gitzhofer F Production of active carbon-supported Fischer-Tropsch nano-catalysts using induction suspension plasma-spray (SPS) technology
30. Le Van K, Luong TTT (2019) Preparation of pore-size controllable activated carbon from rice husk using dual activating agent and its application in supercapacitor. J Chem. https://doi.org/10.1155/2019/4329609
31. Ghanbari F, Moradi M (2017) Application of peroxymonosulfate and its activation methods for degradation of environmental organic pollutants: review. Chem Eng J 310:41–62
32. Wang YR, Chu W (2011) Degradation of a xanthene dye by Fe(II)-mediated activation of Oxone process. J Hazard Mater 186:1455–1461. https://doi.org/10.1016/j.jhazmat.2010.12.033
33. Zhang Y, Huo JB, Yang JCE, Fu ML (2019) Facile fabrication of elastic CoO@graphene aerogel for recycled degradation of chloramphenicol. Mater Lett 240:88–91. https://doi.org/10.1016/j.matlet.2018.12.132
34. Anipsitakis GP, Stathatos E, Dionysiou DD (2005) Heterogeneous activation of Oxone using Co 3O 4. J Phys Chem B 109:13052–13055. https://doi.org/10.1021/jp052166y
35. Yang Y, Jiang J, Lu X et al (2015) Production of sulfate radical and hydroxyl radical by reaction of ozone with peroxymonosulfate: a novel advanced oxidation process. Environ Sci Technol 49:73307339. https://doi.org/10.1021/es506362e
36. Yuan R, Ramjaun SN, Wang Z, Liu J (2011) Effects of chloride ion on degradation of Acid Orange 7 by sulfate radical-based advanced oxidation process: Implications for formation of chlorinated aromatic compounds. J Hazard Mater 196:173–179. https://doi.org/10.1016/j.jhazmat.2011.09.007
37. Antoniou MG, de la Cruz AA, Dionysiou DD (2010) Degradation of microcystin-LR using sulfate radicals generated through photolysis, thermolysis and e- transfer mechanisms. Appl Catal B Environ 96:290–298. https://doi.org/10.1016/j.apcatb.2010.02.013
38. Ling SK, Wang S, Peng Y (2010) Oxidative degradation of dyes in water using Co2+/H2O2 and Co2+/peroxymonosulfate. J Hazard Mater 178:385–389. https://doi.org/10.1016/j.jhazmat.2010.01.091
39. Huang YF, Huang YH (2009) Behavioral evidence of the dominant radicals and intermediates involved in Bisphenol A degradation using an efficient Co2+/PMS oxidation process. J Hazard Mater 167:418–426. https://doi.org/10.1016/j.jhazmat.2008.12.138
40. Pang Y, Kong L, Chen D et al (2020) Facilely synthesized cobalt doped hydroxyapatite as hydroxyl promoted peroxymonosulfate activator for degradation of Rhodamine B. J Hazard Mater. https://doi.org/10.1016/j.jhazmat.2019.121447
41. Dung NT, Thu TV, Van Nguyen T et al (2020) Catalytic activation of peroxymonosulfate with manganese cobaltite nanoparticles for the degradation of organic dyes. RSC Adv 10:3775–3788. https://doi.org/10.1039/c9ra10169a
42. Li H, Wan J, Ma Y et al (2016) Degradation of refractory dibutyl phthalate by peroxymonosulfate activated with novel catalysts cobalt metal-organic frameworks: Mechanism, performance, and stability. J Hazard Mater 318:154–163. https://doi.org/10.1016/j.jhazmat.2016.06.058
43. Erdem H, Erdem M (2020) Synthesis and characterization of a novel activated carbon–supported cobalt catalyst from biomass mixture for tetracycline degradation via persulfate activation. Biomass Convers Biorefinery. https://doi.org/10.1007/s13399-020-00963-z

44. Mahamallik P, Pal A (2020) Photo-Fenton process in Co(II)-adsorbed admicellar soft-template on alumina support for methyl orange degradation. Catal Today 348:212–222. https://doi.org/10.1016/j.cattod.2019.07.045
45. Chen L, Yang S, Zuo X et al (2018) Biochar modification significantly promotes the activity of Co3O4 towards heterogeneous activation of peroxymonosulfate. Chem Eng J 354:856–865. https://doi.org/10.1016/j.cej.2018.08.098
46. Pi Y, Gao H, Cao Y et al (2020) Cobalt ferrite supported on carbon nitride matrix prepared using waste battery materials as a peroxymonosulfate activator for the degradation of levofloxacin hydrochloride. Chem Eng J. https://doi.org/10.1016/j.cej.2019.122377
47. Kang S, Hwang J (2021) CoMn2O4 embedded hollow activated carbon nanofibers as a novel peroxymonosulfate activator. Chem Eng J. https://doi.org/10.1016/j.cej.2020.127158
48. Li L, Wu H, Chen H et al (2020) Heterogeneous activation of peroxymonosulfate by hierarchically porous cobalt/iron bimetallic oxide nanosheets for degradation of phenol solutions. Chemosphere. https://doi.org/10.1016/j.chemosphere.2020.127160
49. Ghanbari F, Moradi M, Gohari F (2016) Degradation of 2,4,6-trichlorophenol in aqueous solutions using peroxymonosulfate/activated carbon/UV process via sulfate and hydroxyl radicals. J Water Process Eng 9:22–28. https://doi.org/10.1016/j.jwpe.2015.11.011
50. Günay T, Çimen Y (2017) Degradation of 2,4,6-trichlorophenol with peroxymonosulfate catalyzed by soluble and supported iron porphyrins. Environ Pollut 231:1013–1020. https://doi.org/10.1016/j.envpol.2017.08.059
51. Tabit R, Amadine O, Essamlali Y et al (2018) Magnetic CoFe2O4 nanoparticles supported on graphene oxide (CoFe2O4/GO) with high catalytic activity for peroxymonosulfate activation and degradation of rhodamine B. RSC Adv 8:1351–1360. https://doi.org/10.1039/c7ra09949e
52. Zhu J, Zhu Z, Zhang H et al (2019) Calcined CoAl-layered double hydroxide as a heterogeneous catalyst for the degradation of acetaminophen and rhodamine B: activity, stability, and mechanism. Environ Sci Pollut Res 26:33329–33340. https://doi.org/10.1007/s11356-019-06390-6
53. Huang C, Wang Y, Gong M et al (2020) A-MnO2/Palygorskite composite as an effective catalyst for heterogeneous activation of peroxymonosulfate (PMS) for the degradation of Rhodamine B. Sep Purif Technol 230:115877. https://doi.org/10.1016/j.seppur.2019.115877
54. Zhao L, Yang D, Ma L et al (2021) An efficient heterogeneous catalyst of FeCo2O4/g-C3N4 composite for catalytic peroxymonosulfate oxidation of organic pollutants under visible light. Colloids Surf A Physicochem Eng Asp. https://doi.org/10.1016/j.colsurfa.2020.125725
55. Zhang D, Li Y, Guo J et al (2021) MOFs-derived magnetic C@Cu–Ni bimetal particles: an efficient peroxymonosulfate activator for 2,4,6-trichlorophenol degradation. Chemosphere. https://doi.org/10.1016/j.chemosphere.2020.129394
56. Zhu B, Yu Y, Ding Y, Ge S (2022) Iron-modified granular sludge biochar-based catalysts for improved Rhodamine B degradation by activating peroxymonosulfate. Biomass Convers Biorefinery. https://doi.org/10.1007/s13399-022-03340-0
57. Chen S, Hu J, Lu L et al (2022) Iron porphyrin-TiO2 modulated peroxymonosulfate activation for efficient degradation of 2,4,6-trichlorophenol with high-valent iron-oxo species. Chemosphere 309:136744. https://doi.org/10.1016/j.chemosphere.2022.136744
58. Wang A, Ni J, Wang W et al (2022) MOF derived Co−Fe nitrogen doped graphite carbon@crosslinked magnetic chitosan Micro−nanoreactor for environmental applications: Synergy enhancement effect of adsorption−PMS activation. Appl Catal B Environ 319:121926. https://doi.org/10.1016/j.apcatb.2022.121926
59. Wang M, Li T, Hou Q et al (2022) Facile one-step preparation of Co and Ce doped TiO2 in visible light PMS activation for PAHs degradation. Chemosphere 308:136360. https://doi.org/10.1016/j.chemosphere.2022.136360
60. Li Y, Zhang S, Qin Y et al (2022) Preparation of cobalt/hydrochar using the intrinsic features of rice hulls for dynamic carbamazepine degradation via efficient PMS activation. J Environ Chem Eng 10:108659. https://doi.org/10.1016/j.jece.2022.108659
61. Wang S, Wang J (2022) Bimetallic and nitrogen co-doped biochar for peroxymonosulfate (Pms) activation to degrade emerging contaminants. SSRN Electron J. https://doi.org/10.2139/ssrn.4273735

Authors and Affiliations

Hakkı Türker Akçay[1] · Adem Demir[2] · Zehra Özçifçi[1] · Tuğrul Yumak[3] · Turgut Keleş[2]

[1] Department of Chemistry, Faculty of Arts and Sciences, Recep Tayyip Erdoğan University, Rize, Turkey

[2] Central Research Laboratory, Application and Research Centre, Recep Tayyip Erdoğan University, Rize, Turkey

[3] Department of Chemistry, Faculty of Arts and Sciences, Sinop University, Sinop, Turkey